Impacting metamaterials: The threshold for wave propagation in holey columns

Sophie Monnery,[1] Shresht Jain,[2,3] Chris Johnson,[3,4] Draga Pihler-Puzović,[2,3] and Finn Box[2,3]
[1]*Institut Jean Le Rond d'Alembert, CNRS UMR7190, Sorbonne Université Paris, 75005 Paris, France*
[2]*Physics of Fluids & Soft Matter, Department of Physics & Astronomy, University of Manchester, Manchester M13 9PL, United Kingdom*
[3]*Manchester Centre for Nonlinear Dynamics, University of Manchester, Manchester M13 9PL, United Kingdom*
[4]*Department of Mathematics, University of Manchester, Manchester M13 9PL, United Kingdom*

(Received 22 January 2024; accepted 24 June 2024; published 16 July 2024)

We study the dynamic deformation of columns containing a periodic array of holes subject to impact loading. When compressed slowly, holey columns buckle beyond a critical compressive strain, and global pattern switching (from circular holes to orthogonal ellipses) occurs instantaneously. In contrast, the dynamic deformation of holey columns is driven by wave propagation; impact induces a compressive wave that buckles the ligaments surrounding a hole, nucleating a sequential pattern switching process. Subsequent void collapse, which ultimately leads to self-contact and topological modification, is driven by the moving boundary. Here, we identify the critical impact velocity above which the compression can no longer be considered quasistatic, and we show that it depends on system size. For dynamic deformations, we show that internal displacements are independent of impact velocity and propagate at the material sound speed, whereas the topological transition wave propagates at a speed that depends on the impact velocity.

DOI: 10.1103/PhysRevMaterials.8.075605

I. INTRODUCTION

Solid structures containing a periodic array of holes are, conceptually, one of the simplest designs of metamaterial. Perforated plates provide a platform for wave control since the holes, or cavities, act as resonator unit cells that interact with incident, transmitted, or surface waves via local resonances associated with hole geometry [1–8]. Acoustic metamaterials exploit the resonances of periodically spaced holes to manipulate wavefront propagation for applications in energy harvesting, signal processing, and sound absorption [1–4]. Metasurfaces and metalenses based on nanohole arrays can focus optical frequencies [5], incident infrared light [6], and surface plasmons [7,8]. The field of flexible mechanical metamaterials, in particular, was kick-started by the discovery that an elastomeric sheet containing an array of circular holes (i.e., a periodically arranged microstructure) exhibits auxetic behavior under compression because its circular holes transform into orthogonal ellipses [9]. The phenomenon has been exploited in the design of photonic [10] and phononic [11] crystals, although research has focused on the programmable buckling mechanics of holey structures under quasistatic loading [12–24]. However, many applications involve dynamic loading; for example, in sports engineering, auxetic foams [25] find application as light-weight impact absorbers in running shoes and protective sports equipment [26,27].

Here we consider soft, holey structures of finite size, subject to impact loading. Holey columns have been studied under impulsive elastic recoil following quasistatic straining and, compared to unstructured materials under the same conditions, these metamaterials were found to enhance energy storage [28–30]. We focus on a different loading strategy, demonstrating that impact can either result in quasistatic buckling or induce sequential wave dynamics and a topological transition that is driven by the moving boundary; see Fig. 1.

Highly deformable mechanical metamaterials subject to pulsatile loading are known to support nonlinear elastic waves [31,32]. These architectures can exhibit amplitude gaps [32–34] enabling the programmable design of mechanical splitters and diodes, and devices for mode focusing and pulse separation [35], but they are typically distinct from systems that exhibit dynamic changes in topology. Topological transition waves are instead associated with moving phase boundaries and domain formation [36–40], and they have been harnessed in flexible metamaterials for rapid reconfiguration and dynamic deployment of three-dimensional structures [41].

By building scaling arguments that balance the timescales of information propagation with the timescales of microstructural deformation, we find the threshold between quasistatic pattern formation and wave propagation in holey structures. We also show that, in contrast to elastic foams [42,43] for which voids similarly constitute a large volume fraction of the material, the nonlinear waves that precede topological change propagate at the material sound speed of the bulk elastomer. In doing so, we demonstrate that dynamic buckling provides an alternative route to pattern formation, as is the case during the impact loading of elastic rods [44–46] and ultrathin sheets at an air-liquid interface [47,48], and in the response of elastic bands to rapid changes in applied tension [49–51].

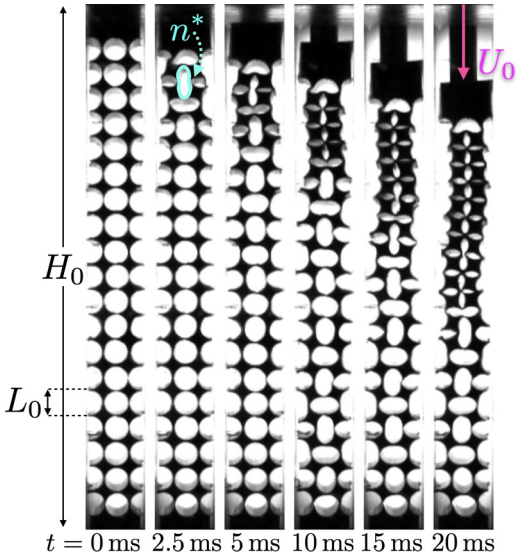

FIG. 1. Dynamic deformation of a holey column. Images of a deforming holey column with $N = 19$ holes (of diameter $D = 8$ mm) following impact at $U_0 = 1.1\,\mathrm{ms}^{-1}$. Sequential pattern switching is seen to nucleate in the second hole from the impacted boundary, $n^* = 2$ (highlighted in cyan), before propagating through the rest of the column.

II. EXPERIMENTS

We fabricated experimental samples from polyvinyl siloxane (Elite Double 22 & 32, Zhermack) with a measured density in the range $\rho = 1160 \pm 50\,\mathrm{kg\,m}^{-3}$ and Poisson's ratio $\nu = 0.47 \pm 0.1$. The Young's modulus of the bulk material was measured to be $270 \leqslant E \leqslant 955 \pm 35$ kPa using an Instron 3345; E was varied within this range by mixing together different ratios of the two grades of elastomer. Unless explicitly stated, data are reported for experiments with columns that contained a periodic array of holes of diameter $D = 8$ mm separated by struts of minimum thickness $w = 0.5$ mm, so that the neighboring holes center-to-center distance (i.e., the length of the unit cell) was $L_0 = D + w = 8.5$ mm. We also performed experiments with columns that had the same L_0, but for which $w = 0.75$ and 1.5 mm and $D = 7.75$ and 7 mm, respectively. The depth of all columns was 16.85 mm while the height depended on the number of holes N in the array, which varied from 7 to 23. At the top and bottom ends of the sample, an extra $l_{\mathrm{ends}} = 12$ mm of solid material free from holes was added to the column, so that its initial height was $H_0 = NL_0 + 2l_{\mathrm{ends}}$.

Columns were placed inside a Perspex holder, whose inner walls were covered in petroleum jelly (Vaseline, Unilever) to prevent solid-solid friction between the column and the container walls. Impact loading was applied by either dropping an impactor (of weight 1 kg) from a height or by catapulting the impactor downwards using a tensioned resistance band. In both cases, the motion of the impactor (a cylindrical rod with a rectangular plate at its head that matches the cross-section of the samples in the top view) was restricted to the vertical direction by guiding rails.

The dynamic deformation of the columns was imaged using a high-speed video camera (FASTCAM Mini UX50, Photron) typically at 4000 fps and with a spatial resolution of 3.1 pixels/mm. The impact speed U_0 was measured from acquired images immediately prior to contact and found to be in the range $0.1 - 5.53\,\mathrm{m\,s}^{-1}$. On timescales of interest here, the impactor did not slow down appreciably.

III. RESULTS

In Fig. 2(a) we present a phase diagram for pattern transformation based on the impact speed and the number of holes in the column. Quasistatic and dynamic pattern formation are differentiated by measuring the position of primary void collapse; for quasistatic deformations, the first hole to collapse is in the middle of the structure and results in global pattern switching. By contrast, dynamic pattern formation is initialized locally by a hole collapse near the loaded end of the structure, which is accelerating and therefore experiencing a greater relative force [Fig. 2(b)]. In finite columns, the first hole to succumb to local buckling, i.e., the first hole to pattern switch, n^*, is expected to be some distance away from the impacted boundary because boundary conditions prevent rotations. Indeed, in our experiments, pattern switching has never been observed in the hole closest to the impacted boundary. However, for larger impact speed, n^* is closer to the impacted boundary [Fig. 2(c)]. The critical threshold for dynamic buckling depends on the number of holes in (and therefore length of) the column and is distinct from the amplitude gap reported in, e.g., [32,33], since even in our low-velocity (quasistatic) experiments the imposed strain is sufficient for pattern switching to occur.

To estimate the threshold impact speed above which dynamic buckling is observed, we recall that a critical strain must be exceeded for a single hole, $\varepsilon_{\mathrm{cr}}^{\mathrm{hole}} = \delta_{\mathrm{cr}}/L_0$, where δ_{cr} is the critical compressive displacement and L_0 is the length of a unit cell. During impact, the top boundary of the column is displaced by a distance $\delta \sim U_0 t$ and a single hole buckles when $\delta \sim \delta_{\mathrm{cr}} \sim U_0 t_{\mathrm{buck}}$, where t_{buck} is the buckling timescale. To distinguish between quasistatic and dynamic buckling, we compare t_{buck} to the time taken for information to propagate through the column, $t_{\mathrm{info}} = H_0/c$, at the speed of sound in the bulk material $c = \sqrt{E/\rho}$. In the limit of quasistatic buckling, $t_{\mathrm{buck}} \gg t_{\mathrm{info}}$ and pattern switching occurs globally. By balancing timescales, $t_{\mathrm{info}} \sim t_{\mathrm{buck}}$, and recalling that $H_0 \sim NL_0$, we find the threshold impact speed, U_{cr}, above which buckling nucleates locally and then propagates,

$$\frac{U_0}{c} \sim \frac{\delta_{\mathrm{cr}}}{H_0} \Rightarrow \frac{U_{\mathrm{cr}}}{c} \sim \frac{\varepsilon_{\mathrm{cr}}^{\mathrm{hole}}}{N}.$$

In Fig. 2(a), we present results for a given hole geometry and material parameters, such that $\varepsilon_{\mathrm{cr}}^{\mathrm{hole}}$ is a constant [20] [measured to be 4.5×10^{-2}; see the Supplemental Material (SM) for further details], and we include a best fit of the form $U_{\mathrm{cr}} \sim N^{-1}$. In Fig. 3 we present results on the threshold velocity for holey columns of different geometries, for which $\varepsilon_{\mathrm{cr}}^{\mathrm{hole}}$ was measured independently (see the SM). These results corroborate the scaling $U_{\mathrm{cr}}/c \sim \varepsilon_{\mathrm{cr}}^{\mathrm{hole}}/N$, demonstrating that the critical threshold velocity is governed by the material properties and length of the column, and the micromechanics of the ligaments surrounding the holes.

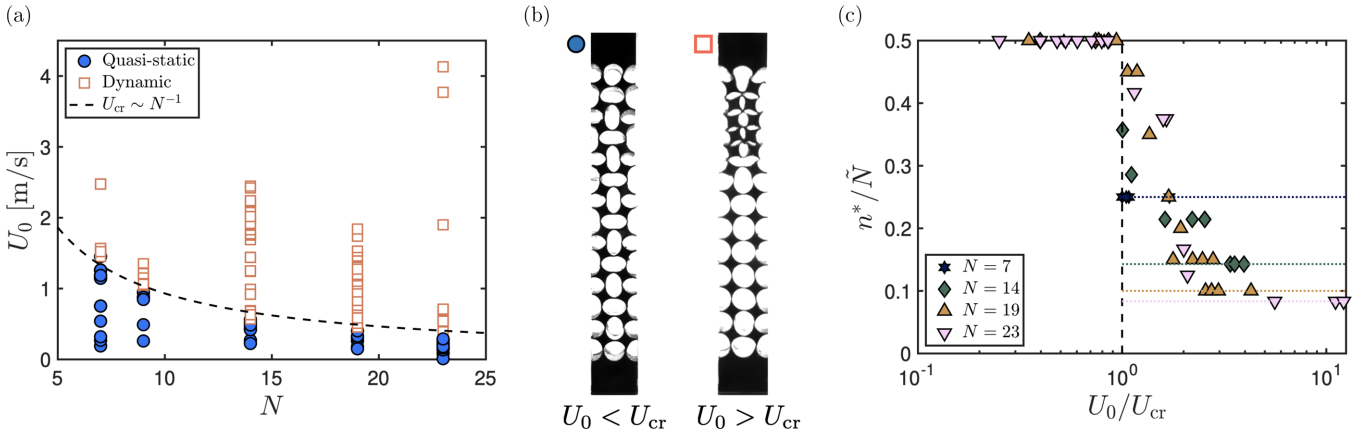

FIG. 2. Critical threshold speed for dynamic buckling. (a) Phase diagram of the mechanical response of a column with N holes to dynamic loading at impact speeds U_0. Circle markers represent a quasistatic response, associated with a global pattern switch that occurs simultaneously across the column and for which the primary void collapse is in the middle of the structure. Square markers represent a dynamic response evidenced by a sequential switching of holes and associated propagation of a buckling wave. The dashed line represents a best fit of the form $U_{cr} \sim N^{-1}$. (b) Typical pattern transformation in a column with $N = 14$ holes for $U_0 < U_{cr}$, when primary void collapse is in the middle of the structure as expected in the quasistatic limit, and for $U_0 > U_{cr}$, when sequential, dynamic buckling occurs; in the images $U_0 = 0.22\,\mathrm{m\,s^{-1}}$ (left) and $U_0 = 2.24\,\mathrm{m\,s^{-1}}$ (right) and $\delta/H_0 = 0.01$. (c) The first hole from the column top to pattern switch, n^*, normalized by $\tilde{N}$, where $\tilde{N} = N$ for columns with even N and $\tilde{N} = N + 1$ for columns with odd N, measured as a function of the scaled impact speed U_0/U_{cr} using data in (a). The dotted lines correspond to $n^* = 2$ in experiments with columns of different length specified using the legend.

The dynamic response of holey columns to impact loading for $U_0 > U_{cr}$ is well visualized from measurements of the eccentricity of the holes as a function of time following impact [Fig. 4(a)]. Here we define the hole eccentricity to be $e = a/b$, where a is the horizontal diameter and b is the vertical diameter of an ellipse fitted to a hole contour in experimental images, such that a circular hole has $e = 1$, while a hole elongated horizontally has $e > 1$ and a hole elongated vertically has $e < 1$. Prior to impact, the holes remain circular, and

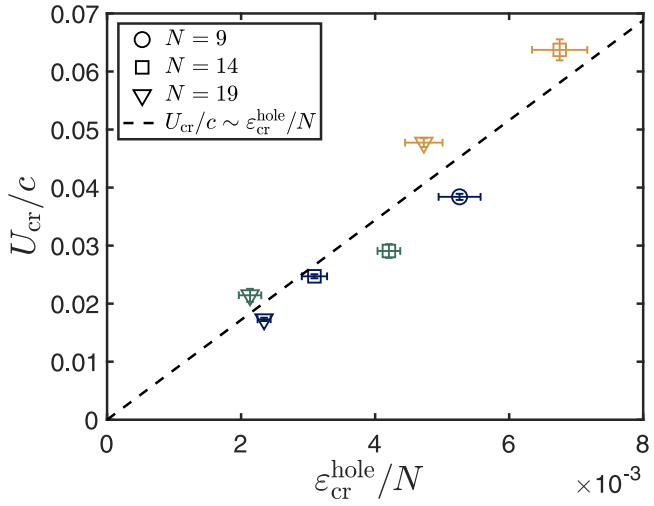

FIG. 3. Scaling the threshold speed with geometry. Threshold speed U_{cr} normalized by $c = \sqrt{E/\rho}$ and measured as a function of $\varepsilon_{cr}^{hole}/N$, where N is the number of holes. The critical strain for a single hole, ε_{cr}^{hole}, depends on the micromechanics of ligaments (see the SM) and, in particular, the minimum ligament width w. Markers shape represents experimental data for different N while the color scheme represents different w, as indicated in the respective legends. The dashed line represents the scaling $U_{cr}/c \sim \varepsilon_{cr}^{hole}/N$.

$e = 1$. The initial deviation from $e = 1$ demarcates the local compression in the column; we observe compression to propagate through the column at a constant rate v_{comp} and measure $e > 1$ for all holes, at early times, implying that the compressive wave squashes circular holes into horizontal ellipses. The subsequent buckling of ligaments leads to pattern switching whereby alternate ellipses switch from a horizontal to a vertical orientation, evidenced by measurements of $e < 1$. The pattern switching process is sequential, propagating through the column at a constant speed v_{buck}, and is henceforth referred to as a buckling wave. Once the hole deformation is sufficient for self-contact to occur, we can no longer measure e; a null measurement demarcates self-contact, and sequential null measurements indicate the propagation of a topological transition wave through the column.

The speeds of the compression, buckling, and self-contact wave are shown in Figs. 4(b)–4(d) as a function of impact speed U_0 for $N = 19$. The propagation of pattern switching and self-contact events was measured by tracking the evolution of the hole eccentricity, while the speed of the compression wave was measured by tracking the initial displacement of horizontal ligaments from their rest position. This was also corroborated by recording the eccentricity of the holes and noting when it first deviated from the value measured prior to impact (see the SM).

Remarkably, compression was found to propagate through the low-density cellular solid at the speed of sound of the bulk material, see Fig. 4(b), independent of impact velocity. We validated this assessment by independently measuring the compressive wave speed c_{exp} in a solid column made from an elastomer with $E = 670\,\mathrm{kPa}$ using particle image velocimetry [dashed lines in Figs. 4(a) and 4(b) and the SM]. We note that this is the rate at which information propagates through the system, rather than the speed at which material points are displaced (which occurred at a fraction of the material sound

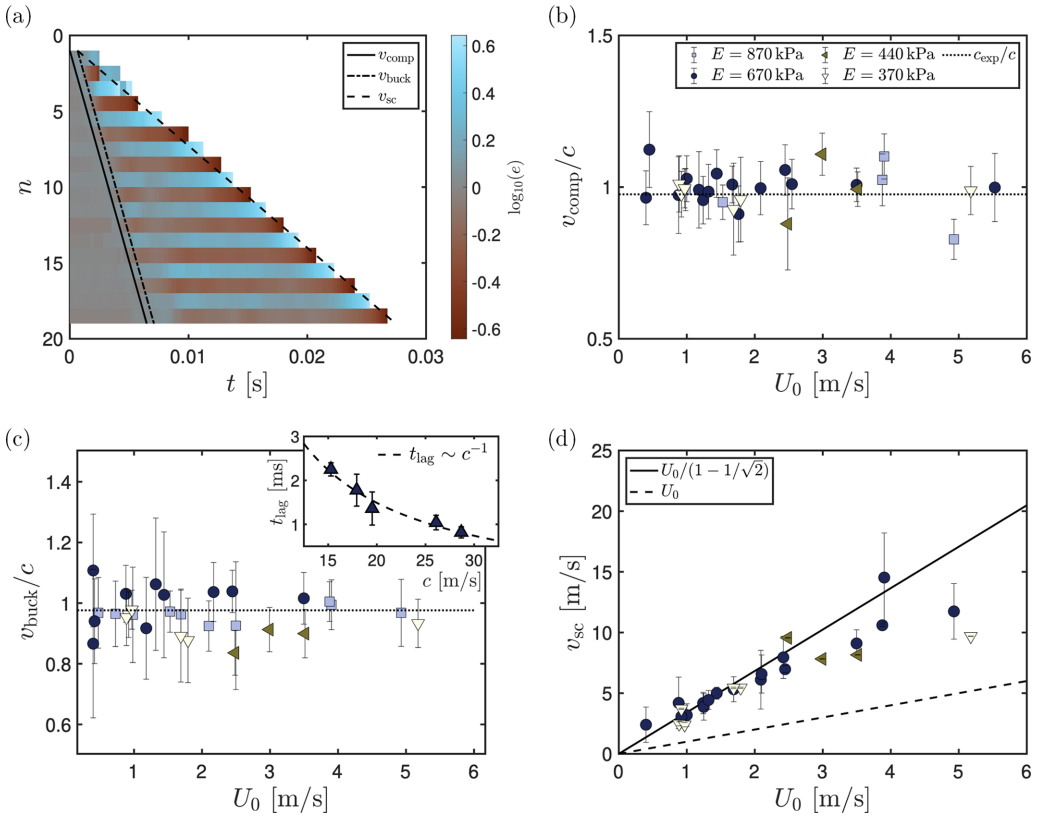

FIG. 4. Wave propagation through holey columns with $N = 19$ holes. (a) Eccentricity e of each hole n in a column measured as a function of time after impact at $t = 0$ at speed $U_0 = 1.53\,\mathrm{m/s}$. Lines represent the propagation of the compressive, buckling, and self-contact waves through the column (as indicated in the legend). (b) Compressive wave speed v_{comp} normalized by the speed of sound in a solid $c = \sqrt{E/\rho}$ as a function of impact speed U_0 for columns made from elastomers with different E. Dotted line was obtained by directly measuring the speed of sound in the material c_{exp}; see the SM. (c) Normalized buckling wave speed v_{buck}/c measured as a function of impact speed U_0 for the same columns as in (b). The inset shows time delay t_{lag} between the onset of compression and buckling waves as a function of the material sound speed c; the dashed line represents the scaling $t_{lag} \sim c^{-1}$ fitted to the experimental data. (d) Self-contact wave speed v_{sc} measured as a function of impact speed U_0 for the same columns as in (b). The solid and dashed lines correspond to the theoretical upper and lower bounds of v_{sc}, respectively.

speed in holey metamaterials in [28,29] that were impulsively released from a prestretched configuration).

The buckling wave also propagates at a rate approximately equal to c, independent of U_0; see Fig. 4(c). The framework of [31,32,52] describes the coupled copropagation of compression and bucking waves as an elastic vector soliton comprised of two polarizations, one of displacement and another of rotation. The waves observed here differ in functional form from those reported in [31,32] because our indentation is dynamic, rather than an impulse. In the case of dynamic compression, the functional form of both compressive and rotational waves is the same (see [53]), and akin to the functional form of the displacement soliton reported in [31,32], whereas application of an impulsive torque generates rotational waves of distinct functional form. The distinction arises because, for dynamic indentation, the moving boundary causes hole eccentricity to change continuously and irreversibly while the deformation is applied.

IV. CONCLUSIONS

The buckling wave was found to lag behind the compressive wave with a time delay that depends on the material sound speed [Fig. 4(c), inset], which can be varied by altering the Young's modulus of the material. This nonzero phase lag suggests that the buckling wave is nucleated by the compressive buckling of the ligaments surrounding a single hole, and that the compressive wave (rather than the moving boundary) is responsible for its onset. Hence, $\delta_{cr}^{hole} \sim ct_{lag}$ from which we recover $t_{lag} \sim L_0/c$ [dashed line in Fig. 4(c), inset].

A consequence of the moving boundary is the subsequent topological transition that results from the sequential self-contact of neighboring holes. The self-contact wave is transmitted through the holey column at a rate that depends on the impact speed U_0, as shown in Fig. 4(d). Our measurements of the self-contact wave speed are bounded by two limits. The lower bound is determined by the speed of the indentor. The upper bound is determined by the geometry of the joints connecting ligaments, and it can be understood using an idealized model in which a unit cell is replaced by four rigid squares that are initially in vertex-to-vertex contact but can rotate as a hinge around these vertices [34,54]. Hence, before void collapse, the maximum distance between the centers of two rotating squares is L_0. This distance is minimal when the squares are in edge-to-edge contact, becoming $L_0/\sqrt{2}$. The distance that the centers are required to move to switch from

a completely open to the closed state is $d = L_0(1 - 1/\sqrt{2})$. The shortest timescale for void collapse is therefore given by the time taken by the indentor to travel a distance d, such that scaling $v_{sc}/L_0 \sim U_0/d$ gives a upper bound for the speed of the self-contact wave $v_{sc} = U_0/(1 - 1/\sqrt{2})$ [solid line in Fig. 4(d)]. That the experimental data are close to this upper bound for $U_0 < 3\,\mathrm{m/s}$ indicates that the bending of ligaments has a negligible influence on the speed of the transition wavefront. Deviation of experimental measurements from this upper bound at larger impact speeds coincides with an observation of greater elastic deformation of the unit cells, meaning that they are no longer well described by the idealized model of rigid squares in vertex-to-vertex contact.

We have demonstrated that the mechanical response of a holey metamaterial to impact loading depends not just on the nondimensional impact speed U_0/c, but on the size of the structure (parametrized by the number of holes N) and the micromechanics of the ligaments, informing appropriate design of low-density, finite-sized impact absorbing structures such as a crumple zone and crash protection equipment. In a given system, modification of the rate of loading is sufficient to alter the route taken during a topological transition between a (low-density, reduced stiffness) "open" state and a (high-density, bulk stiffness) "closed" state. Since the systems under inspection deform elastically, and deformations are reversible, different topologies can be realized in the same system in repeated runs, which provides a degree of engineering control over deformation pathway and timescales, and permits programming of impact mitigation capacity.

The reported experimental data are available in the SM [53].

ACKNOWLEDGMENTS

F.B. would like to acknowledge the Royal Society (URF/R1/211730), and S.M. would like to acknowledge the Erasmus+SMT programme. S.J. acknowledges the support of EPSRC DTP Studentship, UK under Grant No. EP-T517823-1.

The authors declare no conflict of interest, and the funders had no role in the design of the study; in the collection, analyses, or interpretation of data; in the writing of the manuscript; or in the decision to publish the results.

[1] B. Hou, J. Mei, M. Ke, W. Wen, Z. Liu, J. Shi, and P. Sheng, Tuning Fabry-Perot resonances via diffraction evanescent waves, Phys. Rev. B **76**, 054303 (2007).

[2] T. J. Graham, A. P. Hibbins, J. R. Sambles, and T. A. Starkey, Underwater acoustic surface waves on a periodically perforated metal plate, J. Acoust. Soc. Am. **146**, 4569 (2019).

[3] T. A. Starkey, J. D. Smith, A. P. Hibbins, J. R. Sambles, and H. J. Rance, Thin structured rigid body for acoustic absorption, Appl. Phys. Lett. **110**, 041902 (2017).

[4] X.-S. Li, Y.-F. Wang, A.-L. Chen, and Y.-S. Wang, Modulation of out-of-plane reflected waves by using acoustic metasurfaces with tapered corrugated holes, Sci. Rep. **9**, 15856 (2019).

[5] F. M. Huang, N. Zheludev, Y. Chen, and F. J. Garcia de Abajo, Focusing of light by a nanohole array, Appl. Phys. Lett. **90**, 091119 (2007).

[6] S. W. D. Lim, M. L. Meretska, and F. Capasso, A high aspect ratio inverse-designed holey metalens, Nano Lett. **21**, 8642 (2021).

[7] L. Yin, V. K. Vlasko-Vlasov, J. Pearson, J. M. Hiller, J. Hua, U. Welp, D. E. Brown, and C. W. Kimball, Subwavelength focusing and guiding of surface plasmons, Nano Lett. **5**, 1399 (2005).

[8] Z. Liu, J. M. Steele, W. Srituravanich, Y. Pikus, C. Sun, and X. Zhang, Focusing surface plasmons with a plasmonic lens, Nano Lett. **5**, 1726 (2005).

[9] T. Mullin, S. Deschanel, K. Bertoldi, and M. C. Boyce, Pattern transformation triggered by deformation, Phys. Rev. Lett. **99**, 084301 (2007).

[10] X. L. Zhu, Y. Zhang, D. Chandra, S. C. Cheng, J. M. Kikkawa, and S. Yang, Two-dimensional photonic crystals with anisotropic unit cells imprinted from poly (dimethylsiloxane) membranes under elastic deformation, Appl. Phys. Lett. **93**, 161911 (2008).

[11] J.-H. Jang, C. Y. Koh, K. Bertoldi, M. C. Boyce, and E. L. Thomas, Combining pattern instability and shape-memory hysteresis for phononic switching, Nano Lett. **9**, 2113 (2009).

[12] K. Bertoldi, M. C. Boyce, S. Seschanel, S. M. Prange, and T. Mullin, Mechanics of deformation-triggered pattern transformations and superelastic behavior in periodic elastomeric structures, J. Mech. Phys. Solids **56**, 2642 (2008).

[13] K. Bertoldi, P. M. Reis, S. Willshaw, and T. Mullin, Negative Poisson's ratio behaviour induced by an elastic instability, Adv. Mater. **22**, 361 (2010).

[14] T. Mullin, S. Willshaw, and F. Box, Pattern switching in soft cellular solids under compression, Soft Matter **9**, 4951 (2013).

[15] F. Box, R. Bowman, and T. Mullin, Dynamic compression of elastic and plastic cellular solids, Appl. Phys. Lett. **103**, 151909 (2013).

[16] C. Coulais, J. T. B. Overvelde, L. A. Lubbers, K. Bertoldi, and M. van Hecke, Discontinuous buckling of wide beams and metabeams, Phys. Rev. Lett. **115**, 044301 (2015).

[17] D. Pihler-Puzović, A. L. Hazel, and T. Mullin, Buckling of a holey column, Soft Matter **12**, 7112 (2016).

[18] C. Coulais, E. Teomy, K. de Reus, Y. Shokef, and M. van Hecke, Combinatorial design of textured mechanical metamaterials, Nature (London) **535**, 529 (2016).

[19] D. J. Rayneau-Kirkhope and M. A. Dias, Recipes for selecting failure modes in 2-d lattices, Extreme Mech. Lett. **9**, 11 (2016).

[20] C. G. Johnson, U. Jain, A. L. Hazel, D. Pihler-Puzović, and T. Mullin, On the buckling of an elastic holey column, Proc. R. Soc. A **473**, 20170477 (2017).

[21] K. Bertoldi, Harnessing instabilities to design tunable architectured cellular materials, Annu. Rev. Mater. Res. **47**, 51 (2017).

[22] K. Bertoldi, V. Vitelli, J. Christensen, and M. van Hecke, Flexible mechanical metamaterials, Nat. Rev. Mater. **2**, 17066 (2017).
[23] D. Rayneau-Kirkhope, C. Zhang, L. Theran, and M. Dias, Analytic analysis of auxetic metamaterials through analogy with rigid link systems, Proc. R. Soc. A **474**, 2210 (2018).
[24] C. Coulais, C. Kettenis, and M. van Hecke, A characteristic length scale causes anomalous size effects and boundary programmability in mechanical metamaterials, Nat. Phys. **14**, 40 (2018).
[25] M. Parisi, T. Allen, M. Colonna, N. Pugno, and O. Duncan, Indentation and impact response of conventional, auxetic, and shear thickening gel infused auxetic closed cell foam, Smart Mater. Struct. **32**, 074004 (2023).
[26] O. Duncan, T. Shepherd, C. Moroney, L. Foster, P. D. Venkatraman, K. Winwood, T. Allen, and A. Alderson, Review of auxetic materials for sports applications: Expanding options in comfort and protection, Appl. Sci. **8**, 941 (2018).
[27] L. Foster, P. Peketi, T. Allen, T. Senior, O. Duncan, and A. Alderson, Application of auxetic foam in sports helmets, Appl. Sci. **8**, 354 (2018).
[28] X. Liang and A. J. Crosby, Programming impulsive deformation with mechanical metamaterials, Phys. Rev. Lett. **125**, 108002 (2020).
[29] X. Liang and A. J. Crosby, Dynamic recoil in metamaterials with nonlinear interactions, J. Mech. Phys. Solids **162**, 104834 (2022).
[30] X. Liang, H. Fu, and A. J. Crosby, Phase-transforming metamaterial with magnetic interactions, Proc. Natl. Acad. Sci. USA **119**, e2118161119 (2022).
[31] B. Deng, J. R. Raney, V. Tournat, and K. Bertoldi, Elastic vector solitons in soft architected materials, Phys. Rev. Lett. **118**, 204102 (2017).
[32] B. Deng, P. Wang, Q. He, V. Tournat, and K. Bertoldi, Metamaterials with amplitude gaps for elastic solitons, Nat. Commun. **9**, 3410 (2019).
[33] B. Deng, V. Tournat, P. Wang, and K. Bertoldi, Anomalous collisions of elastic vector solitons in mechanical metamaterials, Phys. Rev. Lett. **122**, 044101 (2019).
[34] Y. Li, S. Yan, and H. Li, Wave propagation of 2D elastic metamaterial with rotating squares and hinges, Int. J. Mech. Sci. **217**, 107037 (2022).
[35] B. Deng, C. Mo, V. Tournat, K. Bertoldi, and J. R. Raney, Focusing and mode separation of elastic vector solitons in a 2D soft mechanical metamaterial, Phys. Rev. Lett. **123**, 024101 (2019).
[36] N. Nadkarni, A. F. Arrieta, C. Chong, D. M. Kochmann, and C. Daraio, Unidirectional transition waves in bistable lattices, Phys. Rev. Lett. **116**, 244501 (2016).
[37] H. Yasuda, L. M. Korpas, and J. R. Raney, Transition waves and formation of domain walls in multistable mechanical metamaterials, Phys. Rev. Appl. **13**, 054067 (2020).
[38] L. Jin, R. Khajehtourian, J. Mueller, A. Rafsanjani, V. Tournat, K. Bertoldi, and D. M. Kochmann, Guided transition waves in multistable mechanical metamaterials, Proc. Natl. Acad. Sci. USA **117**, 2319 (2020).
[39] B. Deng, J. R. Raney, K. Bertoldi, and V. Tournat, Nonlinear waves in flexible mechanical metamaterials, J. Appl. Phys. **130**, 040901 (2021).
[40] N. Gorbushin, A. Vainchtein, and L. Truskinovsky, Transition fronts and their universality classes, Phys. Rev. E **106**, 024210 (2022).
[41] A. Zareei, B. Deng, and K. Bertoldi, Harnessing transition waves to realize deployable structures, Proc. Natl. Acad. Sci. USA **117**, 4015 (2020).
[42] K. Attenborough, Acoustical characteristics of porous materials, Phys. Rep. **82**, 179 (1982).
[43] R. F. Lambert, Propagation of sound in highly porous open-cell elastic foams, J. Acoust. Soc. Am. **73**, 1131 (1983).
[44] J. R. Gladden, N. Z. Handzy, A. Belmonte, and E. Villermaux, Dynamic buckling and fragmentation in brittle rods, Phys. Rev. Lett. **94**, 035503 (2005).
[45] B. Audoly and S. Neukirch, Fragmentation of rods by cascading cracks: Why spaghetti does not break in half, Phys. Rev. Lett. **95**, 095505 (2005).
[46] D. Karagiozova and M. Alves, Dynamic elastic-plastic buckling of structural elements: A review, Appl. Mech. Rev. **61**, 040803 (2008).
[47] F. Box, D. O'Kiely, O. Kodio, M. Inizan, A. A. Castrejón-Pita, and D. Vella, Dynamics of wrinkling in ultrathin elastic sheets, Proc. Natl. Acad. Sci. USA **116**, 20875 (2019).
[48] D. O'Kiely, F. Box, O. Kodio, J. Whiteley, and D. Vella, Impact on floating thin elastic sheets: A mathematical model, Phys. Rev. Fluids **5**, 014003 (2020).
[49] R. Vermorel, N. Vandenberghe, and E. Villermaux, Rubber band recoil, Proc. R. Soc. A. **463**, 641 (2007).
[50] F. Box, O. Kodio, D. O'Kiely, V. Cantelli, A. Goriely, and D. Vella, Dynamic buckling of an elastic ring in a soap film, Phys. Rev. Lett. **124**, 198003 (2020).
[51] O. Kodio, A. Goriely, and D. Vella, Dynamic buckling of an inextensible elastic ring: Linear and nonlinear analyses, Phys. Rev. E **101**, 053002 (2020).
[52] B. Deng, J. Li, V. Tournat, P. K. Purohit, and K. Bertoldi, Dynamics of mechanical metamaterials: A framework to connect phonons, nonlinear periodic waves and solitons, J. Mech. Phys. Solids **147**, 104233 (2021).
[53] See Supplemental Material at http://link.aps.org/supplemental/10.1103/PhysRevMaterials.8.075605 for a description of the experimental methods used to measure the material sound speed and to track the propagation of the compression and buckling waves, details of the functional form of the compression and buckling waves and the method by which the critical strain of a single hole was determined, which includes Refs. [55,56].
[54] J. Grima and K. Evans, Auxetic behavior from rotating squares, J. Mater. Sci. Lett. **19**, 1563 (2000).
[55] W. Thielicke and R. Sonntag, Particle image velocimetry for MATLAB: Accuracy and enhanced algorithms in PIVlab, J. Open Source Soft. **9**, 12 (2021).
[56] S. Jain, F. Box, C. Johnson, and D. Pihler-Puzović, Material nonlinearities yield doubly negative holey metamaterials, Extreme Mech. Lett. **64**, 102065 (2023).